ACS APPLIED MATERIALS & INTERFACES

Research Article

www.acsami.org

Nanostructured 2D Diporphyrin Honeycomb Film: Photoelectrochemistry, Photodegradation, and Antibacterial Activity

Yuewu Zhao, Qiuwei Shang, Jiachao Yu, Yuanjian Zhang,* and Songqin Liu*

Jiangsu Province Hi-Tech Key Laboratory for Bio-medical Research, School of Chemistry and Chemical Engineering, Southeast University, Nanjing 211189, P. R. China

Supporting Information

ABSTRACT: Surface patterns of well-defined nanostructures play important roles in fabrication of optoelectronic devices and applications in catalysis and biology. In this paper, the diporphyrin honeycomb film, composed of titanium dioxide, protoporphyrin IX, and hemin (TiO_2/PPIX/Hem), was synthesized using a dewetting technique with the well-defined polystyrene (PS) monolayer as a template. The TiO_2/PPIX/Hem honeycomb film exhibited a higher photoelectrochemical response than that of TiO_2 or TiO_2/PPIX, which implied a high photoelectric conversion efficiency and a synergistic effect between the two kinds of porphyrins. The TiO_2/PPIX/Hem honeycomb film was also a good photosensitizer due to its ability to generate singlet oxygen ($^1O_2$) under irradiation by visible light. This led to the use of diporphyrin TiO_2/PPIX/Hem honeycomb film for the photocatalytic inactivation of bacteria. In addition, the photocatalytic activities of other metal-diporphyrin-based honeycomb films, such as TiO_2/MnPPIX/Hem, TiO_2/CoPPIX/Hem, TiO_2/NiPPIX/Hem, TiO_2/CuPPIX/Hem, and TiO_2/ZnPPIX/Hem, were investigated. The result demonstrated that the photoelectric properties of diporphyrin-based film could be effectively enhanced by further coupling of porphyrin with metal ions. Such enhanced performance of diporphyrin compounds opened a new way for potential applications in various photoelectrochemical devices and medical fields.

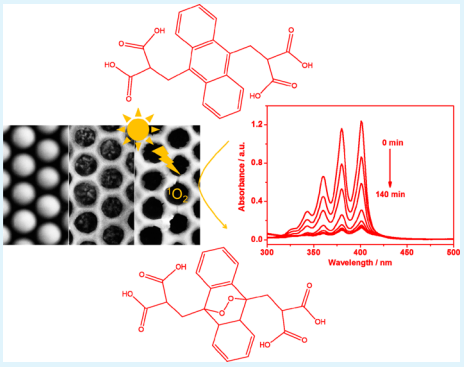

KEYWORDS: *template synthesis, diporphyrin, photoelectrochemistry, synergistic effect, singlet oxygen, antibacterial activity*

1. INTRODUCTION

Recently, porphyrins received much attention due to their attractive optical properties, ultrafast electron injection, and high absorption coefficient to light harvesting.[1−4] These excellent properties led porphyrins to be applied in photoelectrochemical devices to improve photocurrent conversion efficiency.[5−7] Grätzel et al. reported a mesoscopic solar cell using a Co(II/III)tris(bipyridyl) instead of the iodide/triiodide redox shuttle, along with a custom synthesized donor-π-bridge-acceptor zinc porphyrin dye as a sensitizer, which enabled generation of large photocurrents that exceed 12% of the power conversion efficiency.[5] It is believed that energy migration in natural photosynthesis primarily occurred in highly ordered porphyrin-like pigments (chlorophylls).[8−10] This encouraged the development of artificial highly ordered porphyrin-based frameworks for an efficient light-harvesting and energy-transport component. Hupp et al. proposed two kinds of metal−organic frameworks for the highly ordered assembly of two Zn(II) porphyrin struts, respectively, to explore the directional and long-distance exciton migration.[1] The remarkably efficient exciton migration was achieved by enhancing π-conjugation through the addition of two acetylene moieties in the porphyrin molecule, which led to greater Q-band absorption intensity and much faster exciton hopping (energy transfer between adjacent porphyrin struts). On the other hand, the systematic arrangement of multiporphyrin might help in collecting photons with energies across the visible region and form a lowest-excited-state energy gradient that enhanced the efficiency of energy transfer.[11−13] Okada et al. reported a multiporphyrin cascade comprising three varieties of porphyrins, and the intense absorption was observed.[2]

Inspired by the powerful applications of the highly ordered multiporphyrin cascade in solar energy conversion schemes as an efficient light-harvesting and energy-transport component, a diporphyrin honeycomb film composed of titanium dioxide, protoporphyrin IX and hemin (TiO_2/PPIX/Hem) was synthesized. The two-dimensional (2D) honeycomb film as a functional material has been widely used for filtration membranes,[14−16] catalysis,[17] sensors,[18,19] surface-enhanced Raman scattering,[20−22] optoelectronic devices,[23,24] and biology.[25] In general, the honeycomb film could be easily obtained by the template-confined dewetting technique. The well-defined colloidal monolayer templates were achieved by Langmuir−Blodgett,[26] capillary force induced self-assembly,[27,28] electrophoretic deposition,[29] and spin-coating techniques.[30,31] With these templates, a number of 2D nanostructured materials including metal/metal oxides,[32−35] polymers,[36−38] organic/inorganic materials,[39] and hybrid

Received: January 22, 2015
Accepted: May 20, 2015
Published: May 20, 2015

DOI: 10.1021/acsami.5b03254
ACS Appl. Mater. Interfaces 2015, 7, 11783−11791

materials[40,41] have been successfully synthesized. For example, hollow silver spheres with two or three-dimensional ordered structures have been fabricated by employing an ordered colloidal crystal of polystyrene (PS) beads prepared by the micromolding method, and an electroless plating method for depositing the silver coating on the beads.[33] Our previous work synthesized a 3D macroporous Pt catalyst by electrodeposition of Pt into the void spaces of the well-ordered SiO_2 nanosphere template.[32] The resultant macroporous Pt displayed high activity toward the oxidation of methanol. Moreover, as a kind of low-cost active semiconductor, TiO_2 has been used to modify porphyrin derivatives, resulting in enhanced optoelectronic properties.[17,42,43] Herein, a simple and flexible method was used for the rapid fabrication of the well-defined PS monolayer template by floating and reassembly of the PS monolayer at the air/water interface. TiO_2 colloidal nanoparticles were diffused into the void spaces of the template, and the diporphyrin-based TiO_2/PPIX/Hem honeycomb film was thus obtained. Taking into account the increased UV−vis absorption intensity, the photoelectric conversion efficiency and photodynamics of the diporphyrin-based TiO_2/PPIX/Hem honeycomb film was preliminarily examined. A higher photoelectrochemical response and antibacterial activity of the diporphyrin-based honeycomb film were found compared to that only containing porphyrin, due to the synergistic interaction between the two kinds of porphyrins.

2. EXPERIMENTAL SECTION

2.1. Materials. A 2.5 wt % suspension of monodispersed polystyrene spheres (PS) with a diameter of 850 ± 10 nm was purchased from Alfa Aesar Corporation (Beijing, China). 9,10-Anthracenediyl-bis(methylene)dimalonic acid (ABMD) was obtained from Sigma-Aldrich Chemical Corporation (Shanghai, China). *Bacillus subtilis* was obtained from Hubei Qiming Organisms Corporation (Hubei, China). The fluorine-doped tin dioxide (FTO) slices were obtained from Zhuhai Kaivo Optoelectronic Technology Corporation (Zhuhai, China).

The Luria−Bertani (LB) culture medium was prepared as follows: 0.5 g of yeast extract, 1 g of tryptone, and 0.5 g of sodium chloride were thoroughly dissolved in 100 mL of sterilized water. After adjusting the solution pH to 7.0 ± 0.1 by using 1.0 M sodium hydroxide solution, the liquid LB culture medium was obtained. The solid LB culture medium was obtained by the addition of 1.5 g of agar powder into 100 mL of liquid LB culture medium and heated to 90 °C for 30 min.

2.2. Preparation of Diporphyrin Honeycomb Film. FTO slices were cleaned with acetone, ethanol, and deionized water in an ultrasonic bath. The fabrication of the colloidal monolayer film is shown in Figure S1. In a typical process, 10 μL of the PS suspension was spread onto an FTO slice and dried in the air. The slice was then slowly immersed into water to release the PS spheres from FTO and form the close-packed PS spheres array on the surface of deionized water. This phenomenon can be explained by several mechanisms: (i) The PS colloidal possesses an ambivalent behavior, which keeps the spheres trapped at the air/water interface. (ii) Charges exist on the PS spheres surface, which induce the result of electrostatic equilibrium. (iii) The hexagonal structure is the thermodynamic stable position with minimum free energy. Therefore, the close-packed PS spheres array was formed. The floating PS spheres monolayer was collected by a previously cleaned FTO slice. The resulting PS spheres coated FTO slice was finally dried in the air and heated at 110 °C for 15 min to obtain a stable PS template with bright iridescent color on the surface of FTO.

The TiO_2 colloid was prepared by hydrolysis of titanium butoxide according to the literature with slight modifications.[44] Briefly, 30 mL of titanium butoxide was slowly added into 35 mL of anhydrous ethanol under stirring at room temperature to form a homogeneous solution A. A total of 14 mL of acetic acid was added into the mixture of 5 mL of deionized water and 35 mL of anhydrous ethanol to obtain solution B. Then, solution B was slowly dropped into solution A under stirring. The mixture was stirred for another 3 h to obtain the pale yellow TiO_2 colloid.

For fabrication of the diporphyrin honeycomb film, 4 μL of as-prepared TiO_2 colloid was dropped at the edge of the PS template. The diffusion of TiO_2 colloidal nanoparticles into the space of the PS template led to the formation of a cross-linked PS/TiO_2 network structure. Then, 4 μL of 1 mM PPIX in DMSO was dropped on the PS/TiO_2 network film to adsorb PPIX onto the surface of TiO_2 colloidal nanoparticles through bidentate binding interaction between TiO_2 and PPIX. After that, the PS template was removed from PS/TiO_2/PPIX film by immersing the modified FTO slice into the CH_2Cl_2 solution. TiO_2/PPIX honeycomb film was thus obtained. For preparation of TiO_2/PPIX/Hem honeycomb film, the TiO_2/PPIX modified FTO slice was immersed in a 1 mM hemin solution in DMSO for 30 min to allow the hemin molecules to be assembled onto the surface of TiO_2/PPIX honeycomb film through electrostatic and π−π stacking interactions. After washing with DMSO three times, the diporphyrin-based TiO_2/PPIX/Hem honeycomb film was thus obtained. The whole process for preparation of diporphyrin-based TiO_2/PPIX/Hem honeycomb film was illustrated in Scheme 1.

Scheme 1. Schematic of the Fabrication of the Diporphyrin TiO_2/PPIX/Hem Honeycomb Film

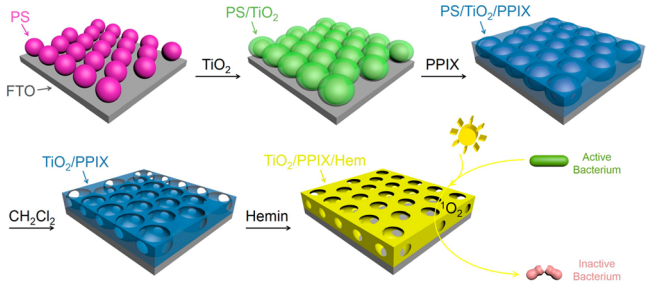

The metalloporphyrins-based honeycomb film was also fabricated using metalloporphyrins instead of PPIX during the TiO_2/PPIX/Hem honeycomb film preparation. Metalloporphyrins were synthesized as follows: an appropriate amount of metal acetate (nickel acetate, manganese acetate, zinc acetate, copper acetate, and cobalt acetate) was dissolved in N,N-dimethylformamide (DMF) to form a 2 mM metal acetate solution. A total of 10 mL of metal acetate solution was mixed with 10 mL of 1 mM PPIX solution and stirred at 120 °C for 4 h in the dark. Then, 20 mL of CH_3OH/H_2O (volume ratio 1:1) was added to the above mixture and kept at 4 °C for 5 h to recrystallize and precipitate metalloporphyrin. The resultant metalloporphyrin precipitation was collected, washed thoroughly with CH_3OH/H_2O and water, and dried in a vacuum at 50 °C for 12 h.

2.3. Apparatus. Photoelectrochemical measurements were carried out with a CHI 660C electrochemical workstation (Chenhua, Shanghai, China) in a conventional three-electrode system composed of the TiO_2/PPIX/Hem modified FTO electrode with an area of 0.64 cm^2 as a working electrode, a saturated calomel electrode (SCE) as a reference electrode, and a Pt wire as a counterelectrode. A white light Xe lamp source of 150 W was used as the irradiation source. The illuminating light intensity was 16 mW cm^{-2}, as estimated by a radiometer.

Morphology and size of the TiO_2/PPIX/Hem honeycomb film were examined on a field-emission scanning electron microscopy (SEM, JEOL JSM-5610LV, Japan). Energy dispersive X-ray spectra (EDS) were taken on a high-resolution transmission electron microscope performed at 200 kV (TEM, JEOL JEM-100S, Japan). X-ray diffraction (XRD, D8 Advance, Bruker, Germany) of the as-prepared TiO_2 was performed with graphite monochromatized Cu Kα radiation (λ = 0.15406 nm), and the data were collected in the 2θ range of 20−80° at a step size of 0.02°. X-ray photoelectron

DOI: 10.1021/acsami.5b03254
ACS Appl. Mater. Interfaces 2015, 7, 11783−11791

spectroscopy (XPS) was acquired using a Kratos Analytical Axis Ultra DLD spectrometer equipped with a monochromatic Al Kα source at 1486.6 eV. UV−vis absorption spectra were recorded on a 2450 UV−visible spectrophotometer (Shimadzu, Japan).

2.4. Antibacterial Activity of TiO_2/PPIX/Hem Honeycomb Film. The bacteria were activated in a minimal medium at 70 °C for 30 min. The medium was composed of an appropriate amount of glass beads, three drops of tween 80, and 1 g of *Bacillus subtilis* seed in 100 mL of sterilized water. Then, 1 mL of activated *Bacillus subtilis* was added to 100 mL of liquid LB culture medium and grown at 25 °C for 12 h to reach the logarithm stage. After that, 10 μL of resultant bacterial solution was dropped onto TiO_2/PPIX/Hem honeycomb film and covered with a cover glass. The resultant FTO slice was illuminated using a 150 W Xe lamp with a light intensity of 1 mW cm^{-2} for 20, 40, 60, 80, and 100 min or incubated in the dark at 25 °C for 100 min. Afterward, the slice was washed with 2 mL of sterilized phosphate buffer solution (PBS, 0.1 M, pH 7.0) to collect bacterial suspension. Then, 10 μL of this bacterial suspension was spread on the solid LB culture medium and incubated at 25 °C for 15 h. The measurements were carried out three times, and the counted average values with statistical deviation were used in the data analysis.

3. RESULTS AND DISCUSSION

The 2D diporphyrin honeycomb film was fabricated using the template-confined dewetting technique.[45] SEM images showed that the PS template on FTO was arranged in a regular close-packed hexagon (Figure 1a and b).[46,47] When TiO_2 colloidal nanoparticles were diffused into the space between PS particles, a network nanostructure was observed (Figure 1c). After binding of porphyrin to TiO_2 nanoparticles through ester-like or bidentate interactions,[3] the PS/TiO_2/PPIX film remained in the same highly ordered topology as PS/TiO_2 itself (Figure 1d). Subsequent to removal of the PS template with CH_2Cl_2 solution, a uniform and smooth TiO_2/PPIX honeycomb structure with a diameter of apertures ranging from 740 to 780 nm was obtained (Figure 1e). Further coupling of hemin through electrostatic and $\pi-\pi$ stacking interactions resulted in TiO_2/PPIX/Hem that maintained the same morphology as the TiO_2/PPIX honeycomb film (Figure 1f). In order to elucidate the detailed structure of the TiO_2/PPIX/Hem honeycomb film, the HRTEM and selected area electron diffraction (SAED) were investigated (Figure S2). The SAED pattern showed diffuse rings indicative of the amorphous state of the TiO_2/PPIX/Hem film. The HRTEM image also confirmed that the specimen was the amorphous structure. X-ray photoelectron spectroscopy (XPS) was performed to characterize the formation of the TiO_2/PPIX/Hem film (Figure S3). The porphyrin displayed two peaks located at 532.7 and 533.9 eV assigned to C═O and C−O, respectively. After the formation of the TiO_2/PPIX/Hem film, an emergence of the peak was observed at 531.1 eV corresponding to Ti−O coordination. All of these results confirmed the formation of the uniform TiO_2/PPIX honeycomb with an amorphous structure.

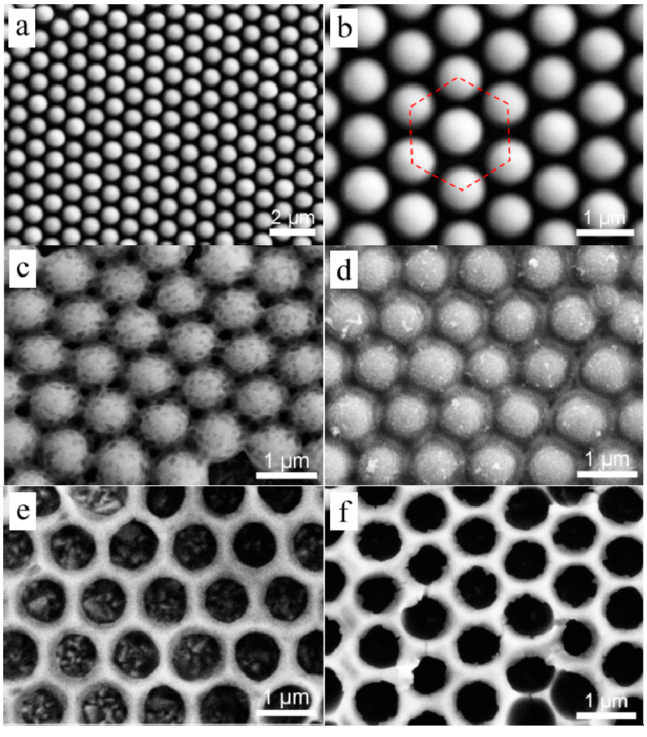

Figure 1. Typical SEM images of (a, b) the PS monolayer colloidal sphere template, (c) the PS/TiO_2 monolayer template, (d) the highly ordered topology with PS/TiO_2/PPIX film, (e) the TiO_2/PPIX ordered porous film after removal of the PS beads, and (f) the as-prepared TiO_2/PPIX/Hem ordered porous film.

The TiO_2 prepared by hydrolysis of titanium butoxide was an amorphous colloid with high purity (strong Tyndall effect shown in Figure S4a, XRD and EDS analysis shown in Figure S4). The formation of the uniform TiO_2/PPIX honeycomb film was dependent on the concentration of TiO_2 colloid. At low colloidal concentration, the SEM images showed fragmentary honeycomb nanopatterns (Figure S5a and b). As the volume ratio of TiO_2/C_2H_5OH was increased to 1:4, the TiO_2/PPIX honeycomb film was successfully obtained after removal of the polymer beads (Figure 1e). With a further increase of the TiO_2 colloid concentration, there was almost no integrated honeycomb film in the final products as seen in Figure S5d. During the drying process, the colloid loses moisture with uneven shrinkage, which makes it easy to break into multiple pieces. These experiments indicated that the as-prepared TiO_2 colloid diluted with ethanol in a proportion of 4:1 was the suitable coating concentration for making the honeycomb film. This was possibly due to the decreased viscosity and increased fluidity of the TiO_2 colloid solution, which disturbed the electrostatic interactions between the same PS spheres.[48]

PPIX could be bound to the PS/TiO_2 film by ester-like or bidentate interactions between TiO_2 nanoparticles and the carboxylic groups on porphyrins. Previous studies demonstrated that the organic porphyrin had ultrafast electron injection and a high absorption coefficient for light harvesting,[3,42] which could be evaluated by the photocurrent measurements. As shown in Figure 2, after PPIX loading, the PS/TiO_2/PPIX film modified FTO showed a large anodic photocurrent of 85 nA at an applied potential of −0.1 V under photoexcitation with a white light source (Xe lamp; Figure 2, curve d). In addition, the PS template modified FTO showed a very small photocurrent of 3.0 nA, while with the FTO substrate, the PS/TiO_2 modified FTO slices showed a photocurrent of 4.5 nA (Figure 2, curves a and c). When PPIX was directly dropped onto the FTO slice, the spontaneous $\pi-\pi$ aggregation of porphyrin was a major reason for the formation of unwanted irregular aggregates (Figure S6b), and a photocurrent of 50 nA (Figure S7b) was obtained under the same conditions. Obviously, the presence of PPIX enhanced the photoexcitation of electrons transferring from PS/TiO_2/PPIX to the FTO electrode; the uniformly dispersed PPIX effectively improved the light-absorbing area and hence increased the photocurrent readout. After removal of PS, the

DOI: 10.1021/acsami.5b03254
ACS Appl. Mater. Interfaces 2015, 7, 11783−11791

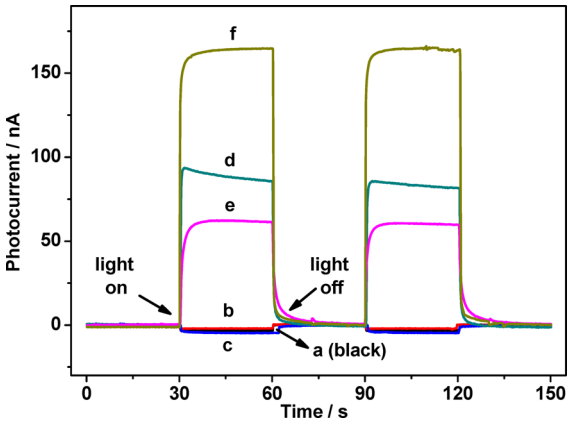

Figure 2. Photocurrent intensity in 0.1 M PBS of (a) FTO electrode, (b) PS monolayer modified FTO electrode, (c) PS/TiO_2 modified FTO electrode, (d) PS/TiO_2/PPIX film modified FTO electrode, (e) TiO_2/PPIX film modified FTO electrode after the dissolution of PS in CH_2Cl_2 solution, (f) TiO_2/PPIX/Hem honeycomb film modified FTO electrode. The working potential was −0.1 V and a Xe lamp with a light intensity of 16 mW cm^{-2}.

TiO_2/PPIX showed an anodic photocurrent of 62 nA, which was slightly lower than that of the PS/TiO_2/PPIX film but still larger than that of PPIX irregular nanospecies. The decrease of photocurrent was possibly due to granular PPIX partly released from the nanocomposites during removal of PS with a solvent. Moreover, the anodic photocurrent of the TiO_2/PPIX honeycomb film was very stable. TiO_2/PPIX showed a photocurrent of 62 nA and no significant attenuation with an illumination time of 0−10 min. The PPIX irregular nanospecies directly assembled on the FTO slice easily; therefore, the formation of the TiO_2/PPIX honeycomb film enhanced the efficiency of the photoexcitation electron transfer and the stability of the photocatalyst.

In addition, the coating of hemin to form the TiO_2/PPIX/Hem honeycomb film could further amplify the photocurrent readout to 164 nA (Figure 2, curve f), which was 2.6 times larger than that of the TiO_2/PPIX honeycomb film. The photocurrent increase after hemin coupling might come from the synergistic effect between two porphyrins, which could be evaluated by the UV−vis measurements. As shown in Figure 3a, the UV−vis absorption spectra of TiO_2 exhibited an increasing absorption from 391 to 328 nm and reached a plateau at 328 nm (Figure 3a, curve a). The UV−vis absorption spectrum of PPIX showed a strong Soret absorption at 407 nm together with four weak Q bands at 505, 541, 574, and 629 nm (Figure 3a, curve b), which resulted from the p−p* transition between the highest occupied molecular orbital and the lowest unoccupied molecular orbital. For the TiO_2/PPIX honeycomb film, a wide range absorption spectrum emerged from the 486 to 350 nm range (Figure 3a, curve c). The Soret band of PPIX became wider and weaker than PPIX itself, while the Q bands located at the same position as PPIX increased the absorption intensity. The difference of UV−vis absorption spectra between PPIX and the TiO_2/PPIX honeycomb film could be attributed to the dentate binding of TiO_2 and carboxyl groups of PPIX.[49] With the addition of hemin, the TiO_2/PPIX/Hem honeycomb film further increased the Q-band intensity compared to the TiO_2/PPIX honeycomb film, indicating a synergistic effect between two porphyrins. The synergistic effect between two porphyrins increased the UV−vis absorption intensity and also led to the enhancement of photocurrent readout.

The mechanism for the generation of anodic photocurrent is summarized in Figure 4.[3,50,51] Under irradiation with light, the electron−hole pairs of TiO_2 were generated by excitation and the charge separation. Then, two opposite electron transfer processes occurred: the electron transfer from the conduction band (CB) of TiO_2 to FTO produced an anodic photocurrent, while the other transferred electrons from the FTO electrode to the valence band (VB) of TiO_2, which resulted in a cathodic photocurrent. At a potential of −0.1 V (vs. SCE), the electron transfer from the FTO electrode to the VB of TiO_2 was predominant, and the cathodic photocurrent was observed. In the presence of PPIX, the electrons could transfer from excited PPIX to the CB of TiO_2 due to the higher energy level of the excited state of PPIX. Subsequently, the electrons transferred to the FTO electrode and generated the anodic photocurrent. The photoelectric properties of hemin were similar to those of PPIX; it could effectively transferred electrons from the excited state of hemin to the CB of TiO_2. These results further enhanced the anodic photocurrent.

Porphyrins were also used as photosensitizers to efficiently convert ground state molecular oxygen ($^3O_2$) to singlet oxygen ($^1O_2$) under irradiation by visible light. The highly reactive $^1O_2$ generated could lead to photodynamic inactivation of microorganisms and lethal damage to cancer cells.[52,53] To investigate the ability of diporphyrin-based TiO_2/PPIX/Hem to generate $^1O_2$, 9,10-anthracenediyl-bis(methylene)dimalonic acid

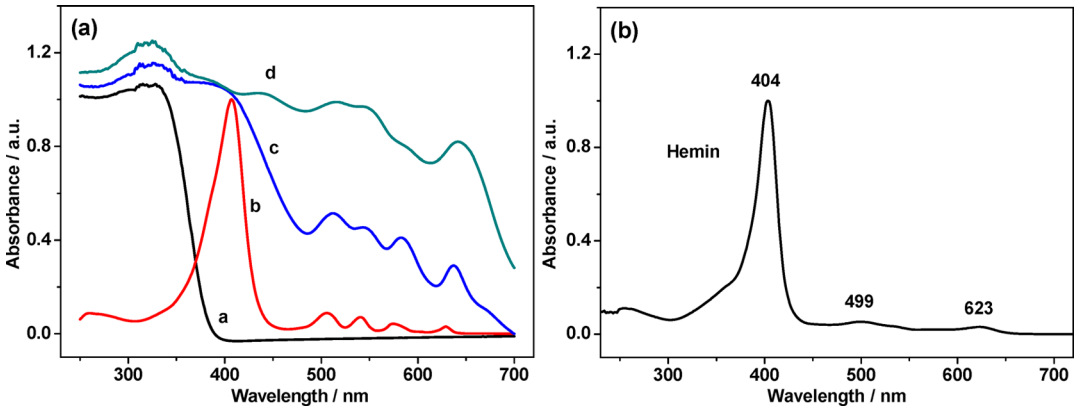

Figure 3. UV−vis absorption spectra of (a) TiO_2 (curve a), PPIX (curve b), TiO_2/PPIX (curve c), TiO_2/PPIX/Hemin (curve d) and (b) the Hemin.

DOI: 10.1021/acsami.5b03254
ACS Appl. Mater. Interfaces 2015, 7, 11783−11791

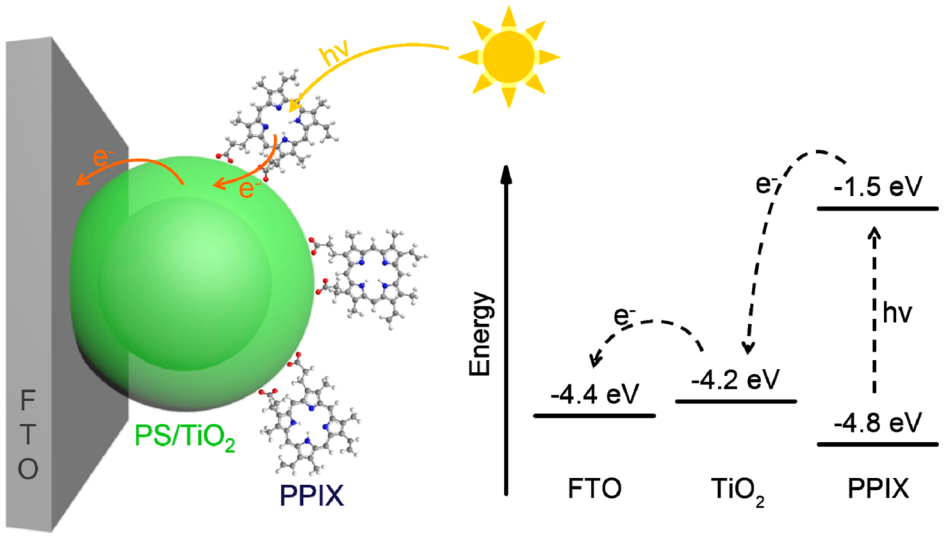

Figure 4. Schematic illustration of the electron transfer process of the PS/TiO_2/PPIX modified FTO electrode upon illumination.

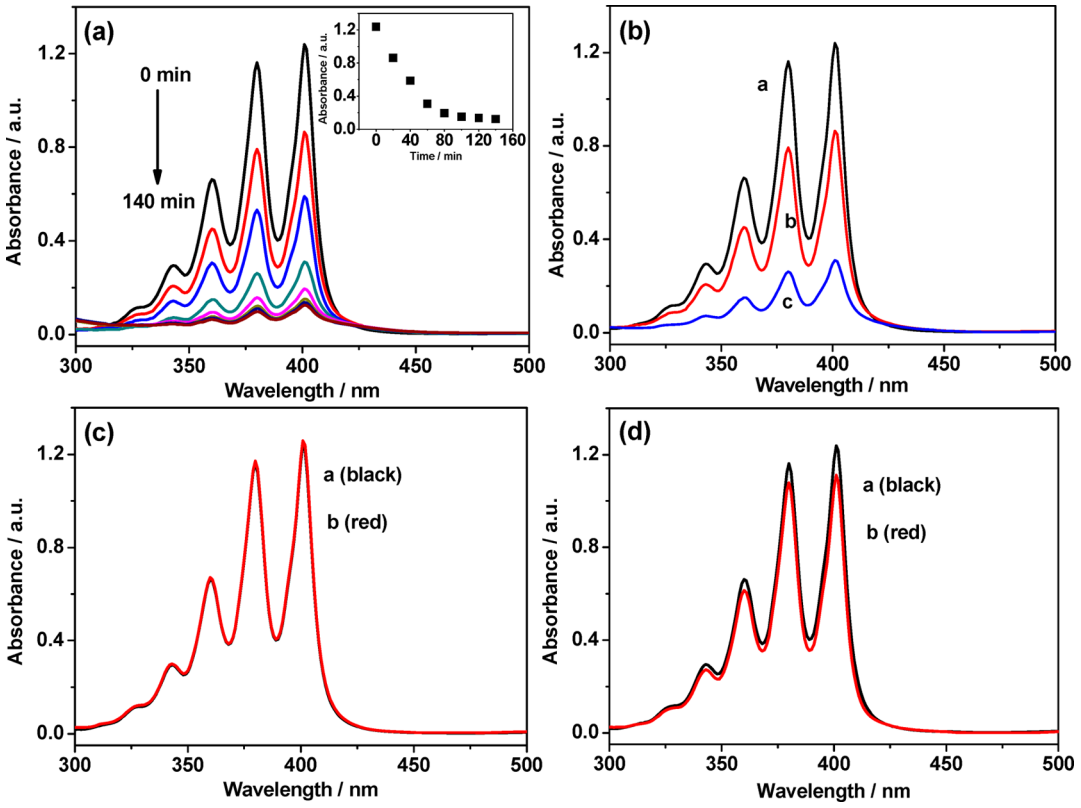

Figure 5. (a) Absorption of the ABMD (0.5 mmol L^{-1}) caused by singlet oxygen generated from diporphyrin-based TiO_2/PPIX/Hem film with an illumination time of 0−140 min. The inset is the absorption intensity of the ABMD at 401 nm as a function of illumination time, 0−140 min. (b) Obtained UV−vis absorption of ABMD (0.5 mmol L^{-1}) in the presence of TiO_2/PS (curve a), TiO_2/PPIX (curve b), and TiO_2/PPIX/Hem (curve c) with an illumination time of 1 h. (c) Absorption intensity in the dark for 1 h, indicating the necessity of illumination. (d) Absorption intensity under the N_2-saturated condition for 1 h, indicating the necessity of O_2.

(ABMD) was used as a probe to react with $^1O_2$ to yield an endoperoxide, which quenched the UV−vis absorption of the probe.[54,55] The photobleaching was carried out using a 150 W Xe lamp with a light intensity of 16 mW cm^{-2} as a light source in 0.5 mM ABMD solution in DMSO. As seen in Figure 5a, the characteristic peaks of ABMD at 401, 380, 360, and 343 nm could be observed. In the presence of TiO_2/PPIX/Hem honeycomb film, the UV−vis absorption intensity of ABMD gradually decreased with the increase of illumination time and reached a steady state at about 80 min (Inset in Figure 5a). Control experiments were performed using TiO_2/PS film and TiO_2/PPIX honeycomb film instead of TiO_2/PPIX/Hem honeycomb film under the same conditions. The TiO_2/PS film displayed no activity to generate $^1O_2$ (Figure 5b, curve a). The TiO_2/PPIX honeycomb film also displayed the decrease of the absorption intensity of ABMD (Figure 5b, curve b);

DOI: 10.1021/acsami.5b03254
ACS Appl. Mater. Interfaces 2015, 7, 11783−11791

however, its intensity was 2.5 times smaller than that of TiO_2/PPIX/Hem honeycomb film under the same conditions. This is similar to 2.6 times difference of the photocurrent measurement for TiO_2/PPIX and TiO_2/PPIX/Hem honeycomb film. This confirmed that the diporphyrin-based TiO_2/PPIX/Hem film exhibited much higher photosensitizing efficiency than the TiO_2/PPIX film. The formation of diporphyrin-based TiO_2/PPIX/Hem film effectively improved the photodynamic activation to generate $^1O_2$ under UV illumination. On the other hand, the absorption of ABMD kept the same shape and intensity as ABMD when the TiO_2/PPIX/Hem honeycomb film and ABMD were mixed together without illumination with a Xe lamp (Figure 5c). While a slight decrease of UV adsorption intensity was observed for the N_2-saturated solution containing TiO_2/PPIX/Hem honeycomb film and ABMD under illumination (Figure 5d). This slight decrease of UV adsorption intensity of ABMD was from the residual oxygen in solution. All these results confirmed that the illumination and O_2 were the essential factors for the generation of $^1O_2$.

The $^1O_2$ photoinduced by the diporphyrin-based TiO_2/PPIX/Hem film could cause the inactivation of microorganisms, which was demonstrated by an antibacterial activity assay.[56] It can be seen in Figure 6 that the fraction of surviving *Bacillus subtilis* decreased 16% under visible light irradiation as the TiO_2 colloid existed alone (Figure 6, curve a). For the TiO_2/PPIX film (Figure 6, curve b), the disinfect fraction of *Bacillus subtilis* was 35% after visible light irradiation within 60 min and 50% at 100 min. However, in the case of the diporphyrin-based TiO_2/PPIX/Hem film (Figure 6, curve c), the disinfect fraction of *Bacillus subtilis* reached 82% within 60 min, and 88% at 100 min. The disinfect fraction of *Bacillus subtilis* for TiO_2/PPIX/Hem film was 2.3 times larger than that for TiO_2/PPIX film, which suggested that the diporphyrin-based TiO_2/PPIX/Hem film had more efficient antibacterial ability than TiO_2/PPIX film. Without visible light irradiation, the disinfect fractions of *Bacillus subtilis* were 7% and 5% for TiO_2/PPIX/Hem and TiO_2/PPIX films, respectively (Figure S9). Thus, this confirmed that $^1O_2$ photoinduced by porphyrins under visible light effectively resulted in the photosensitizing inactivation of bacteria.

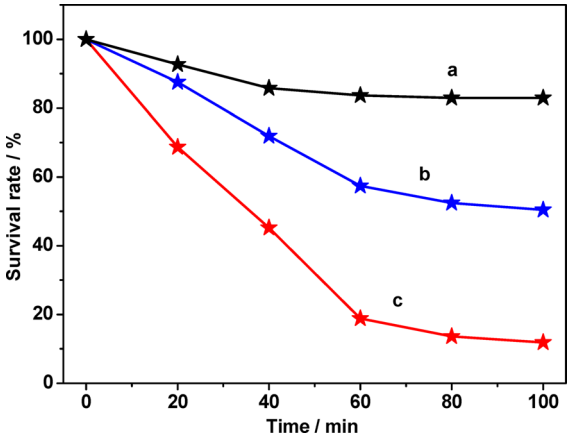

Figure 6. Fraction of surviving *Bacillus subtilis* in the presence of TiO_2 colloid (curve a), TiO_2/PPIX (curve b), and TiO_2/PPIX/Hem (curve c) as a function of the Xe lamp with a light intensity of 1 mW cm^{-2} for 100 min.

To further illustrate the effective synergy between two porphyrins, metalloporphyrins, NiPPIX, MnPPIX, ZnPPIX, CuPPIX, and CoPPIX were prepared and used (Figures S10 and S11), instead of PPIX, to form a diporphyrin honeycomb film. The resultant ability to generate $^1O_2$ was investigated. As shown in Figure 7, all the metalloporphyrin-based diporphyrin honeycomb films showed much higher efficiency to the generated $^1O_2$ than PPIX and metalloporphyrin alone. This confirmed that the synergistic effect of two porphyrins effectively enhanced their photoactivities. Meanwhile, the strength of the synergistic effect could be calculated by a UV−vis absorption degradation rate of ABMD using the following expression: $D = (Ab_1 - Ab_2)/Ab_0$, where Ab_0 was the initial absorption intensity of ABMD, Ab_1 was the absorption intensity of ABMD with TiO_2/MPPIX (TiO_2/MnPPIX, TiO_2/CoPPIX, TiO_2/NiPPIX, TiO_2/CuPPIX, and TiO_2/ZnPPIX film) as a photosensitizer for 1 h, and Ab_2 was the absorption intensity of ABMD with TiO_2/MPPIX/Hem for 1 h. The calculated degradation rates of ABMD were presented in Figure 8. All these observations indicated that diporphyrin honeycomb film had an effective synergistic effect for generation of $^1O_2$ under visible light, and the TiO_2/NiPPIX/Hem film had the highest synergistic effect.

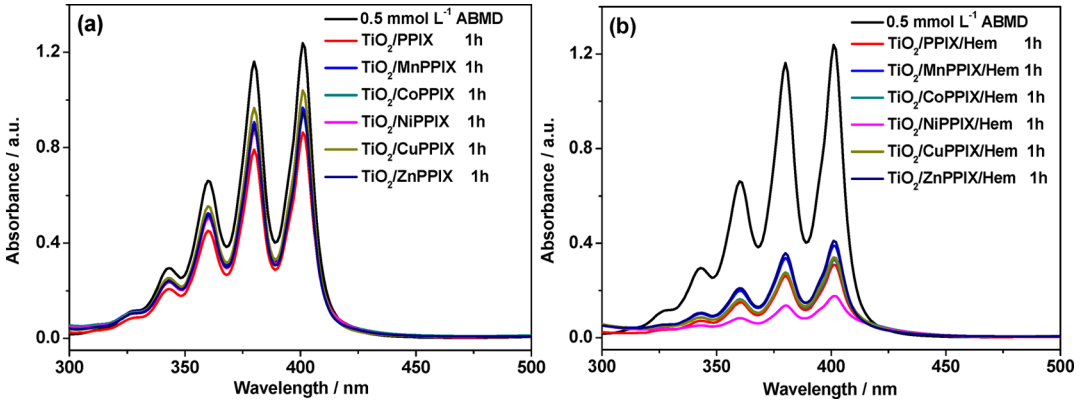

Figure 7. (a) Absorption of the ABMD (0.5 mmol L^{-1}) caused by singlet oxygen generated from TiO_2/PPIX, TiO_2/MnPPIX, TiO_2/CoPPIX, TiO_2/NiPPIX, TiO_2/CuPPIX, and TiO_2/ZnPPIX films with illumination time of 1 h. (b) Absorption of the ABMD (0.5 mmol L^{-1}) caused by singlet oxygen generated from TiO_2/PPIX/Hem, TiO_2/MnPPIX/Hem, TiO_2/CoPPIX/Hem, TiO_2/NiPPIX/Hem, TiO_2/CuPPIX/Hem, and TiO_2/ZnPPIX/Hem films with an illumination time of 1 h. The Xe lamp with a light intensity of 16 mW cm^{-2}.

DOI: 10.1021/acsami.5b03254
ACS Appl. Mater. Interfaces 2015, 7, 11783−11791

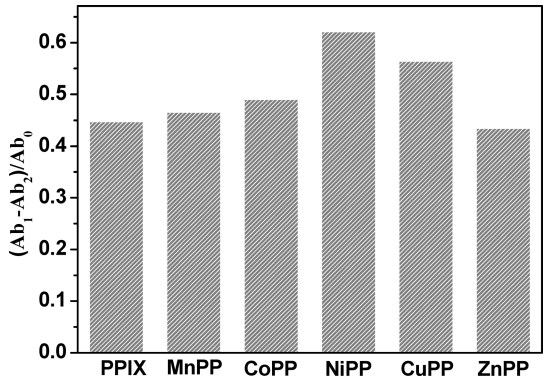

Figure 8. Histogram of the calculated synergistic effect by UV−vis absorption degradation rate of ABMD. $D = (Ab_1 - Ab_2)/Ab_0$, where Ab_0 is the initial absorption intensity of ABMD, Ab_1 is the absorption intensity of ABMD with TiO_2/PPIX (TiO_2/MnPPIX, TiO_2/CoPPIX, TiO_2/NiPPIX, TiO_2/CuPPIX, and TiO_2/ZnPPIX films) as photocatalytic for 1 h, and Ab_2 is the absorption intensity of ABMD with TiO_2/PPIX/Hem (TiO_2/MnPPIX/Hem, TiO_2/CoPPIX/Hem, TiO_2/NiPPIX/Hem, TiO_2/CuPPIX/Hem, and TiO_2/ZnPPIX/Hem films) as photocatalytic for 1 h.

4. CONCLUSIONS

In summary, through the well-defined PS monolayer template dewetting technique, diporphyrin-based TiO_2/PPIX/Hem honeycomb film was successfully synthesized. The PS and TiO_2 colloid solutions play important roles in obtaining the honeycomb film during the formation progress. A higher solar-energy conversion efficiency and synergistic effect has been confirmed regarding the diporphyrin-based TiO_2/PPIX/Hem honeycomb film. Antibacterial activity assays indicate that these TiO_2/PPIX/Hem honeycomb films have efficient antibacterial activities under visible light, indicating that the diporphyrin compounds have a stronger capacity to produce $^1O_2$ due to the synergistic effect. Other diporphyrin-based films (TiO_2/MnPPIX/Hem, TiO_2/CoPPIX/Hem, TiO_2/NiPPIX/Hem, TiO_2/CuPPIX/Hem, and TiO_2/ZnPPIX/Hem) were prepared and compared for the ability to generate $^1O_2$ under visible light; the results demonstrate that the photoelectric properties of diporphyrin-based film could be effectively enhanced. All of these results demonstrated that the diporphyrin-based TiO_2/PPIX/Hem honeycomb film had a higher photoelectric conversion efficiency, strong photodegradation ability, and effective antibacterial activity. Furthermore, the simple and flexible strategy could also be suitable for other materials. Such ordered pore array materials can be used for photoelectric sensors, the photocatalytic reaction, and biological medicine fields.

■ ASSOCIATED CONTENT

Supporting Information

Strategy and characterizations of the ordered PS monolayer colloidal sphere film. SEM, EDS, XRD, and photographs demonstrate that the PS as a template and TiO_2 colloid solution as a cross-linking agent play important roles in obtaining the highly ordered topology with honeycomb film. UV−vis absorption spectral and EDS spectrum confirmed the successful preparation of metalloporphyrin. Some antibacterial activity assays. The Supporting Information is available free of charge on the ACS Publications website at DOI: 10.1021/acsami.5b03254.

■ AUTHOR INFORMATION

Corresponding Authors

*Tel: 86-25-52090613. Fax: 86-25-52090618. E-mail: yuanjian.zhang@seu.edu.cn.

*Tel: 86-25-52090613. Fax: 86-25-52090618. E-mail: liusq@seu.edu.cn.

Notes

The authors declare no competing financial interest.

■ ACKNOWLEDGMENTS

We gratefully acknowledge the National Natural Science Foundation of China (grant nos. 21375014 and 21175021), the Social Development Project of Suzhou (ZXY 2012027), the Funding of Jiangsu Innovation Program for Graduate Education (KYLX 0163), and the Fundamental Research Funds for the Central Universities.

■ REFERENCES

(1) Son, H. J.; Jin, S. Y.; Patwardhan, S.; Wezenberg, S. J.; Jeong, N. C.; So, M.; Wilmer, C. E.; Sarjeant, A. A.; Schatz, G. C.; Snurr, R. Q.; Farha, O. K.; Wiederrecht, G. P.; Hupp, J. T. Light-Harvesting and Ultrafast Energy Migration in Porphyrin-Based Metal-Organic Frameworks. *J. Am. Chem. Soc.* **2013**, *135*, 862−869.

(2) Uetomo, A.; Kozaki, M.; Suzuki, S.; Yamanaka, K.; Ito, O.; Okada, K. Efficient Light-Harvesting Antenna with a Multi-Porphyrin Cascade. *J. Am. Chem. Soc.* **2011**, *133*, 13276−13279.

(3) Tu, W. W.; Dong, Y. T.; Lei, J. P.; Ju, H. X. Low-Potential Photoelectrochemical Biosensing Using Porphyrin-Functionalized TiO_2 Nanoparticles. *Anal. Chem.* **2010**, *82*, 8711−8716.

(4) Jin, C. S.; Lovell, J. F.; Chen, J.; Zheng, G. Ablation of Hypoxic Tumors with Dose-Equivalent Photothermal, but Not Photodynamic, Therapy Using a Nanostructured Porphyrin Assembly. *ACS Nano* **2013**, *7*, 2541−2550.

(5) Yella, A.; Lee, H. W.; Tsao, H. N.; Yi, C.; Chandiran, A. K.; Nazeeruddin, M. K.; Diau, E. W. G.; Yeh, C. Y.; Zakeeruddin, S. M.; Grätzel, M. Porphyrin-Sensitized Solar Cells with Cobalt (II/III)-Based Redox Electrolyte Exceed 12% Efficiency. *Science* **2011**, *334*, 629−634.

(6) Hasobe, T.; Imahori, H.; Fukuzumi, S.; Kamat, P. V. Light Energy Conversion Using Mixed Molecular Nanoclusters. Porphyrin and C_{60} Cluster Films for Efficient Photocurrent Generation. *J. Phys. Chem. B* **2003**, *107*, 12105−12112.

(7) Lee, C. W.; Lu, H. P.; Lan, C. M.; Huang, Y. L.; Liang, Y. R.; Yen, W. N.; Liu, Y. C.; Lin, Y. S.; Diau, E. W. G.; Yeh, C. Y. Novel Zinc Porphyrin Sensitizers for Dye-Sensitized Solar Cells: Synthesis and Spectral, Electrochemical, and Photovoltaic Properties. *Chem.—Eur. J.* **2009**, *15*, 1403−1412.

(8) Barber, Y.; Andersson, B. Revealing the Blueprint of Photosynthesis. *Nature* **1994**, *370*, 31−34.

(9) Umena, Y.; Kawakami, K.; Shen, J. R.; Kamiya, N. Crystal Structure of Oxygen-Evolving Photosystem II at a Resolution of 1.9 Å. *Nature* **2011**, *473*, 55−60.

(10) Blankenship, R. E. *Molecular Mechanisms of Photosynthesis*; Blackwell: Oxford, 2002.

(11) Devadoss, C.; Bharathi, P.; Moore, J. S. Energy Transfer in Dendritic Macromolecules: Molecular Size Effects and the Role of an Energy Gradient. *J. Am. Chem. Soc.* **1996**, *118*, 9635−9644.

(12) Hippius, C.; Stokkum, I. H. M.; Gsänger, M.; Groeneveld, M. M.; Williams, R. M.; Würthner, F. Sequential FRET Processes in Calix[4]arene-Linked Orange-Red-Green Perylene Bisimide Dye Zigzag Arrays. *J. Phys. Chem. C* **2008**, *112*, 2476−2486.

(13) Diring, S.; Puntoriero, F.; Nastasi, F.; Campagna, S.; Ziessel, R. Star-Shaped Multichromophoric Arrays from Bodipy Dyes Grafted on Truxene Core. *J. Am. Chem. Soc.* **2009**, *131*, 6108−6110.

(14) Wan, L. S.; Li, J. W.; Ke, B. B.; Xu, Z. K. Ordered Microporous Membranes Templated by Breath Figures for Size-Selective Separation. *J. Am. Chem. Soc.* **2012**, *134*, 95−98.

DOI: 10.1021/acsami.5b03254
ACS Appl. Mater. Interfaces 2015, 7, 11783−11791

(15) Cong, H. L.; Wang, J. L.; Yu, B.; Tang, J. G. Preparation of a Highly Permeable Ordered Porous Microfiltration Membrane of Brominated Poly(phenylene oxide) on an Ice Substrate by the Breath Figure Method. *Soft Matter* **2012**, *8*, 8835−8839.
(16) Gugliuzza, A.; Aceto, M. C.; Macedonio, F.; Drioli, E. Water Droplets as Template for Next-Generation Self-Assembled Poly(etheretherketone) with Cardo Membranes. *J. Phys. Chem. B* **2008**, *112*, 10483−10496.
(17) Pessoni, L.; Lacombe, S.; Billon, L.; Brown, R.; Save, M. Photoactive, Porous Honeycomb Films Prepared from Rose Bengal-Grafted Polystyrene. *Langmuir* **2013**, *29*, 10264−10271.
(18) Song, Y. Y.; Zhang, D.; Gao, W.; Xia, X. H. Nonenzymatic Glucose Detection by Using a Three-Dimensionally Ordered, Macroporous Platinum Template. *Chem.—Eur. J.* **2005**, *11*, 2177−2182.
(19) Kim, J.; Ng, T. N.; Kim, W. S. Highly Sensitive Tactile Sensors Integrated with Organic Transistors. *Appl. Phys. Lett.* **2012**, *101*, 103308.
(20) Tessier, P. M.; Velev, O. D.; Kalambur, A. T.; Lenhoff, A. M.; Rabolt, J. F.; Kaler, E. W. Structured Metallic Films for Optical and Spectroscopic Applications via Colloidal Crystal Templating. *Adv. Mater.* **2001**, *13*, 396−400.
(21) Kong, L.; Dong, R.; Ma, H.; Hao, J. Au NP Honeycomb-Patterned Films with Controllable Pore Size and Their Surface-Enhanced Raman Scattering. *Langmuir* **2013**, *29*, 4235−4241.
(22) Zhang, Y. J.; Gao, W. T.; Yang, S.; Liu, S. S.; Zhao, X. Y.; Gao, M.; Wang, Y. X.; Yang, J. H. Nanogaps in 2D Ag-Nanocap Arrays for Surface-Enhanced Raman Scattering. *J. Raman Spectrosc.* **2013**, *44*, 1666−1670.
(23) Wang, X. D.; Summers, C. J.; Wang, Z. L. Large-Scale Hexagonal-Patterned Growth of Aligned ZnO Nanorods for Nano-optoelectronics and Nanosensor Arrays. *Nano Lett.* **2004**, *4*, 423−426.
(24) Ma, H. M.; Cui, J. W.; Chen, J. F.; Hao, J. C. Self-Organized Polymer Nanocomposite Inverse Opal Films with Combined Optical Properties. *Chem.—Eur. J.* **2011**, *17*, 655−660.
(25) Manabe, K.; Nishizawa, S.; Shiratori, S. Porous Surface Structure Fabricated by Breath Figures that Suppresses Pseudomonas aeruginosa Biofilm Formation. *ACS Appl. Mater. Interfaces* **2013**, *5*, 11900−11905.
(26) Reculusa, S.; Ravaine, S. Synthesis of Colloidal Crystals of Controllable Thickness through Langmuir-Blodgett Technique. *Chem. Mater.* **2003**, *15*, 598−605.
(27) Vlasov, Y. A.; Bo, X. Z.; Sturm, J. C.; Norris, D. J. On-Chip Natural Assembly of Silicon Photonic Bandgap Crystals. *Nature* **2001**, *414*, 289−293.
(28) Wong, S.; Kitaev, V.; Ozin, G. A. Colloidal Crystal Films: Advances in Universality and Perfection. *J. Am. Chem. Soc.* **2003**, *125*, 15589−15598.
(29) Marín-Suárez, M.; Medina-Rodríguez, S.; Ergeneman, O.; Pané, S.; Fernández-Sánchez, J. F.; Nelson, B. J.; Fernández-Gutiérrez, A. Electrophoretic Deposition as a New Approach to Produce Optical Sensing Films Adaptable to Microdevices. *Nanoscale* **2014**, *6*, 263−271.
(30) Jiang, P.; McFarland, M. J. Large-Scale Fabrication of Wafer-Size Colloidal Crystals, Macroporous Polymers and Nanocomposites by Spin-Coating. *J. Am. Chem. Soc.* **2004**, *126*, 13778−13786.
(31) Yang, S. K.; Cai, W. P.; Kong, L. C.; Lei, Y. Surface Nanometer-Scale Patterning in Realizing Large-Scale Ordered Arrays of Metallic Nanoshells with Well-Defined Structures and Controllable Properties. *Adv. Funct. Mater.* **2010**, *20*, 2527−2533.
(32) Chen, C. L.; Li, Y.; Liu, S. Q. Fabrication of Macroporous Platinum Using Monodisperse Silica Nanoparticle Template and Its Application in Methanol Catalytic Oxidation. *J. Electroanal. Chem.* **2009**, *632*, 14−19.
(33) Chen, Z.; Zhan, P.; Wang, Z. L.; Zhang, J. H.; Zhang, W. Y.; Ming, N. B.; Chan, C. T.; Sheng, P. Two- and Three-Dimensional Ordered Structures of Hollow Silver Spheres Prepared by Colloidal Crystal Templating. *Adv. Mater.* **2004**, *16*, 417−422.
(34) Cao, B. Q.; Cai, W. P.; Sun, F. Q.; Li, Y.; Lei, Y.; Zhang, L. D. Fabrication of Large-Scale Zinc Oxide Ordered Pore Arrays with Controllable Morphology. *Chem. Commun.* **2004**, 1604−1605.
(35) Shin, J. H.; Kang, J. H.; Jin, W. M.; Park, J. H.; Cho, Y. S.; Moon, J. H. Facile Synthesis of TiO_2 Inverse Opal Electrodes for Dye-Sensitized Solar Cells. *Langmuir* **2011**, *27*, 856−860.
(36) Zhu, L. W.; Ou, Y.; Wan, L. S.; Xu, Z. K. Polystyrenes with Hydrophilic End Groups: Synthesis, Characterization, and Effects on the Self-Assembly of Breath Figure Arrays. *J. Phys. Chem. B* **2014**, *118*, 845−854.
(37) Zhang, Z.; Hughes, T. C.; Gurr, P. A.; Blencowe, A.; Uddin, H.; Hao, X. J.; Qiao, G. G. The Behaviour of Honeycomb Film Formation from Star Polymers with Various Fluorine Content. *Polymer* **2013**, *54*, 4446−4454.
(38) Fukuhira, Y.; Yabu, H.; Ijiro, K.; Shimomura, M. Interfacial Tension Governs the Formation of Self-Organized Honeycomb-Patterned Polymer films. *Soft Matter* **2009**, *5*, 2037−2041.
(39) Wong, K. H.; Davis, T. P.; Barner-Kowollik, C.; Stenzel, M. H. Gold-Loaded Organic/Inorganic Nanocomposite Honeycomb Membranes. *Aust. J. Chem.* **2006**, *59*, 539−543.
(40) Li, L.; Zhong, Y. W.; Ma, C. Y.; Li, J.; Chen, C. K.; Zhang, A. J.; Tang, D. L.; Xie, S. Y.; Ma, Z. Honeycomb-Patterned Hybrid Films and Their Template Applications via A Tunable Amphiphilic Block Polymer/Inorganic Precursor System. *Chem. Mater.* **2009**, *21*, 4977−4983.
(41) Sun, W.; Shao, Z.; Ji, J. Particle-Assisted Fabrication of Honeycomb-Structured Hybrid Films via Breath Figures Method. *Polymer* **2010**, *51*, 4169−4175.
(42) Hasobe, T.; Fukuzumi, S.; Hattori, S.; Kamat, P. V. Shape- and Functionality-Controlled Organization of TiO_2-Porphyrin-C_{60} Assemblies for Improved Performance of Photochemical Solar Cells. *Chem.—Asian J.* **2007**, *2*, 265−272.
(43) Wang, Y. R.; Liu, Y.; Li, G. H.; Hao, J. C. Porphyrin-Based Honeycomb Films and Their Antibacterial Activity. *Langmuir* **2014**, *30*, 6419−6426.
(44) Li, X. G.; Liu, C. P.; Xing, W.; Lu, T. H. Development of Durable Carbon Black/Titanium Dioxide Supported Macrocycle Catalysts for Oxygen Reduction Reaction. *J. Power Sources* **2009**, *193*, 470−476.
(45) Yang, S. K.; Xu, F.; Ostendorp, S.; Wilde, G.; Zhao, H. P.; Lei, Y. Template-Confined Dewetting Process to Surface Nanopatterns: Fabrication, Structural Tunability, and Structure-Related Properties. *Adv. Funct. Mater.* **2011**, *21*, 2446−2455.
(46) Xiao, J. Y.; Yang, L.; Luo, Y. H.; Li, D. M.; Meng, Q. B. A Rapid and Scalable Strategy to High Quality Inverse Opal Tin Dioxide Porous Films. *J. Mater. Chem. C* **2013**, *1*, 5450−5453.
(47) Lai, K. Y.; Lin, Y. R.; Wang, H. P.; He, J. H. Synthesis of Anti-Reflective and Hydrophobic Si Nanorod Arrays by Colloidal Lithography and Reactive Ion Etching. *CrystEngComm* **2011**, *13*, 1014−1017.
(48) Harzallah, O. A.; Dupuis, D. Rheological Properties of Suspensions of TiO_2 Particles in Polymer Solutions. 1. Shear Viscosity. *Rheol. Acta* **2003**, *42*, 10−19.
(49) Tu, W. W.; Lei, J. P.; Ding, L.; Ju, H. X. Sandwich Nanohybrid of Single-Walled Carbon Nanohorns-TiO_2-Porphyrin for Electrocatalysis and Amperometric Biosensing towards Chloramphenicol. *Chem. Commun.* **2009**, 4227−4229.
(50) Zhao, W. W.; Ma, Z. Y.; Xu, J. J.; Chen, H. Y. In Situ Modification of a Semiconductor Surface by an Enzymatic Process: A General Strategy for Photoelectrochemical Bioanalysis. *Anal. Chem.* **2013**, *85*, 8503−8506.
(51) Li, L.; Duan, L.; Xu, Y. H.; Gorlov, M.; Hagfeldt, A.; Sun, L. C. A Photoelectrochemical Device for Visible Light Driven Water Splitting by a Molecular Ruthenium Catalyst Assembled on Dye-Sensitized Nanostructured TiO_2. *Chem. Commun.* **2010**, *46*, 4227−4229.
(52) DeRosa, M. C.; Crutchley, R. J. Photosensitized Singlet Oxygen and Its Applications. *Coord. Chem. Rev.* **2002**, *233*−*234*, 351−371.

DOI: 10.1021/acsami.5b03254
ACS Appl. Mater. Interfaces 2015, 7, 11783−11791

(53) Dolmans, D. E.; Fukumura, D.; Jain, R. K. Photodynamic Therapy for Cancer. *Nat. Rev. Cancer* **2003**, *3*, 380−387.
(54) Soares, M. V.; Oliveira, M. R.; Santos, E. P.; Gitirana, L. B.; Barbosa, G. M.; Quaresma, C. H.; Ricci-Júnior, E. Nanostructured Delivery System for Zinc Phthalocyanine: Preparation, Characterization, and Phototoxicity Study Against Human Lung Adenocarcinoma A549 Cells. *Int. J. Nanomed.* **2011**, *6*, 227−238.
(55) Zhao, B. Z.; Yin, J. J.; Bilski, P. J.; Chignell, C. F.; Roberts, J. E.; He, Y. Y. Enhanced Photodynamic Efficacy towards Melanoma Cells by Encapsulation of Pc4 in Silica Nanoparticles. *Toxicol. Appl. Pharmacol.* **2009**, *241*, 163−172.
(56) Kim, D. S.; Kwak, S. Y. Photocatalytic Inactivation of *E. coli* with a Mesoporous TiO_2 Coated Film Using the Film Adhesion Method. *Environ. Sci. Technol.* **2009**, *43*, 148−151.

DOI: 10.1021/acsami.5b03254
ACS Appl. Mater. Interfaces 2015, 7, 11783−11791